Enhancement of Heat Dissipation in Ultraviolet Light-Emitting Diodes by a Vertically Oriented Graphene Nanowall Buffer Layer

Haina Ci, Hongliang Chang, Ruoyu Wang, Tongbo Wei,* Yunyu Wang, Zhaolong Chen, Yuanwei Sun, Zhipeng Dou, Zhiqiang Liu,* Jinmin Li, Peng Gao,* and Zhongfan Liu*

For III-nitride-based devices, such as high-brightness light-emitting diodes (LEDs), the poor heat dissipation of the sapphire substrate is deleterious to the energy efficiency and restricts many of their applications. Herein, the role of vertically oriented graphene (VG) nanowalls as a buffer layer for improving the heat dissipation in AlN films on sapphire substrates is studied. It is found that VG nanowalls can effectively enhance the heat dissipation between an AlN film and a sapphire substrate in the longitudinal direction because of their unique vertical structure and good thermal conductivity. Thus, an LED fabricated on a VG-sapphire substrate shows a 37% improved light output power under a high injection current (350 mA) with an effective 3.8% temperature reduction. Moreover, the introduction of VG nanowalls does not degrade the quality of the AlN film, but instead promotes AlN nucleation and significantly reduces the epilayer strain that is generated during the cooling process. These findings suggest that the VG nanowalls can be a good buffer layer candidate in III-nitride semiconductor devices, especially for improving the heat dissipation in high-brightness LEDs.

The III-nitride semiconductors, such as GaN and AlN, have been widely used for light emitting diodes (LEDs) due to their wide band gaps, high breakdown voltage, and high saturation velocities of electrons.[1–4] In particular, nitride-based LEDs in ultraviolet (UV) luminescent devices have exhibited broad application prospects.[5–7] Despite significant progress in LEDs

in recent years, the problem of heat dissipation still remains,[8] particularly for high-brightness LED devices with large chip areas and large driving currents, which severely degrade the optoelectronic performance (low light output power and poor saturation phenomenon) of LEDs. In recent years, researchers have proposed various approaches to improve the heat dissipation, such as flip-chip packaging,[9–11] thin-film technology,[12,13] and substrate-replacement.[14] For example, flip-chip packaging relies on a sapphire-free thermal path, where the generated heat can be dissipated through the solder to the heat sink. However, the improvement in heat dissipation is usually small because of the poor thermal conductivity between the solder and heat sink. For thin-film technology, the sapphire substrate is first removed by a laser lift-off technique, then the remaining structure is transferred to a high thermally conducting substrate (e.g., a Cu or Si substrate). The laser lift-off and transfer process increases the complexity, and more importantly, inevitable damage occurs during transfer. Due to the rather poor thermal conductivity of sapphire (35 W mK^{-1}), scientists have reported the fabrication of LEDs on bulk GaN or SiC substrates with high

H. Ci, R. Wang, Z. Chen, Prof. P. Gao, Prof. Z. Liu
Center for Nanochemistry (CNC)
Beijing Science and Engineering Center for Nanocarbons
Beijing National Laboratory for Molecular Sciences
College of Chemistry and Molecular Engineering
Academy for Advanced Interdisciplinary Studies
Peking University
Beijing 100871, P. R. China
E-mail: p-gao@pku.edu.cn; zfliu@pku.edu.cn
H. Chang, Prof. T. Wei, Y. Wang, Prof. Z. Liu, Prof. J. Li
State Key Laboratory of Solid-State Lighting
Institute of Semiconductors
Chinese Academy of Sciences
Beijing 100083, P. R. China
E-mail: tbwei@semi.ac.cn; lzq@semi.ac.cn

Prof. T. Wei, Prof. Z. Liu, Prof. J. Li
Center of Materials Science and Optoelectronics Engineering
University of Chinese Academy of Sciences
Beijing 100049, P. R. China
Y. Sun, Z. Dou, Prof. P. Gao
Electron Microscopy Laboratory, and International Center
for Quantum Materials
School of Physics
Peking University
Beijing 100871, P. R. China
Prof. P. Gao, Prof. Z. Liu
Beijing Graphene Institute (BGI)
Beijing 100095, P. R. China
Prof. P. Gao
Collaborative Innovation Centre of Quantum Matter
Beijing 100871, P. R. China

ADVANCED
SCIENCE NEWS
www.advancedsciencenews.com

ADVANCED
MATERIALS
www.advmat.de

thermal conductivities. However, the high cost of GaN and SiC significantly increases the cost of production and thus restricts their wide application. To date, sapphire substrates have been the main substrates used for LED fabrication. It is important to improve the heat dissipation capabilities of sapphire substrates by directly combining proper and valid materials with high thermal conductivities through a low-cost method that has a high production yield.

Indeed, graphene has a high thermal conductivity and high structural stability, enabling its many applications as a coating material for heat dissipation.[15–20] Due to the two-dimensional (2D) structure based on weak van der Waals interactions between graphene layers, the thermal conductivity of graphene is anisotropic, that is, it has a great ability to transfer heat along the in-plane direction (ab direction) but a much poorer ability along the out-of-plane direction (c-direction, [001]).[21,22] Therefore, for a few layers of graphene, heat is mainly transferred through the interfacial layers that are in direct or close contact with the heat source, while those layers far away from the heat source contribute little to the total heat transfer due to the limited thermal conductivity along the c-direction. Compared to common horizontally oriented graphene, the vertically oriented graphene nanosheets[23] have exhibited good thermal transport in both the vertical and horizontal directions due to their three-dimensional (3D) structure and unique vertical orientation,[24] which should effectively promote heat dissipation between a III-nitride semiconductor film and a sapphire substrate and can be supposed to improve the energy efficiency of LEDs.

Herein, we first demonstrate a method for growing high-quality single crystal AlN on a sapphire substrate by using of vertically oriented graphene (VG) nanowalls as a buffer layer. Growth of high quality III-nitride films with low stress and dislocation density is crucial for the semiconductor industry. Especially, for GaN-based UV-LEDs, AlN is usually used as the template layer for the epitaxial of GaN layer and thus the quality of the AlN template layer is essential for epitaxial growth of high-quality GaN to enable high-efficiency UV-LEDs.[25,26]

In our work, the VG nanowalls are directly grown on the sapphire substrate via a low-cost plasma-enhanced chemical vapor deposition (PECVD) method that is highly scalable. Because of their unique vertical structure and excellent thermal conductivity, VG nanowalls can efficiently promote the dissipation of heat generated under irradiation from a light source and thus reduce the operating temperature. In addition, the VG nanowall layer serves two other purposes: it acts as a nucleation site promoting uniform AlN film formation and provides a buffer layer to release the strain between AlN and sapphire generated by the large lattice and thermal mismatches,[27,28] which is helpful for enhancing the energy efficiency. Furthermore, the VG nanowall buffer layer does not degrade the quality of the AlN film. Therefore, this versatile approach provides a new strategy for the application of nitride semiconductor devices, particularly for LEDs with high brightness and high efficiency.

In contrast to the common horizontal graphene layer, vertical graphene nanowalls have a unique 3D structure that enable us to make use of their excellent vertical thermal conductivity to enhance the heat dissipation in LED applications. **Figure 1**a schematically depicts the design. First, VG nanowalls are grown by plasma enhanced chemical vapor deposition (PECVD) at low temperature (≈580 °C) on a (0001) sapphire substrate. More details of the growth process and XPS elemental analysis about VG nanowalls are described in Figures S1 and S2, Supporting Information. The as-grown graphene is almost perpendicular to the substrate, with numerous edge defects, which are mainly induced by the electric field during plasma generation.[29–32] The exposed sharp edges, non-stacking morphology, and large surface-to-volume ratio of graphene can provide a sufficient number of edge defects as sites for AlN nucleation. Then, a 2.0-µm thick AlN film is grown on the VG-sapphire substrate by a one-step high-temperature metal-organic chemical vapor deposition (MOCVD) process. Finally, for the obtained AlN-VG-Al_2O_3 structures, the VG nanowalls exhibit good heat dissipation under illumination.

Figure 1b–e shows representative scanning electron microscopy (SEM), Raman, atomic force microscopy (AFM), and transmission electron microscopy (TEM) images of the as-grown VG nanowalls. From the SEM image in Figure 1b, it can clearly be seen that the VG nanowalls partially cover the surface of the sapphire substrate (the light areas represent the vertical graphene nanowalls and dark areas represent the bare sapphire substrate). The AFM image in Figure 1d shows the distributions of the VG nanosheets with a density of approximately 81 µm^{-2}. The average height of a VG nanosheet is ≈20.5 ± 5.0 nm, as confirmed by the height profile inset in Figure 1d. Raman spectroscopy of the VG nanowalls, shown in Figure 1c, presents characteristic Raman peaks at 1357 cm^{-1} (D band), 1592 cm^{-1} (G band), and 2713 cm^{-1} (2D band),[33] suggesting relatively high crystallinity of the graphene grown at low temperature. In these nanostructures, individual nanosheets usually have lateral dimensions of ≈0.12 ± 0.02 micrometers and a thickness of only several nanometers, consisting of 8–10 layers. The TEM in Figure 1e shows the curved edge of a single VG nanowall.

The vertically oriented graphene nanowalls exhibit a large number of edge defects, which can act as nucleation sites for AlN growth. The cross-section TEM images of AlN nucleation on VG nanowall-sapphire substrate can be seen in Figures S3 and S4, Supporting Information. Therefore, we can effectively control the density of AlN nucleation by tuning the density of the VG nanowalls, that is, the lowest density of AlN nucleation occurs on bare sapphire and higher densities of AlN nucleation occur on sapphire substrates with higher densities of VG nanowalls (**Figure 2**a–g). By simply using one-step MOCVD growth instead of a traditional two-step MOCVD process, a smooth AlN film can be obtained easily, as displayed in the SEM image in Figure 2h. The AFM image in Figure 2i and the inset height profile show that the surface of the as-grown AlN film is atomically flat, with a measured root mean square (RMS) roughness of 1.8 Å over an area of 1.5 µm × 1.5 µm.

The detailed X-ray diffraction (XRD) rocking curve characterization results are shown in Figure S5, Supporting Information. The full width at half maximum (FWHM) values of the (002) and (102) peaks are 329.2 and 569.6 arcs, and the calculated defect densities of screw dislocations and edge dislocations are 2.36×10^8 and 3.22×10^9 cm^{-2}, which could meet the requirements for LED applications.[34] In contrast, a smooth AlN film cannot be obtained on the bare sapphire substrate by using the same procedure, as shown in Figure S6, Supporting Information. This AlN film growth method can effectively shorten the

**ADVANCED
SCIENCE NEWS**
www.advancedsciencenews.com

**ADVANCED
MATERIALS**
www.advmat.de
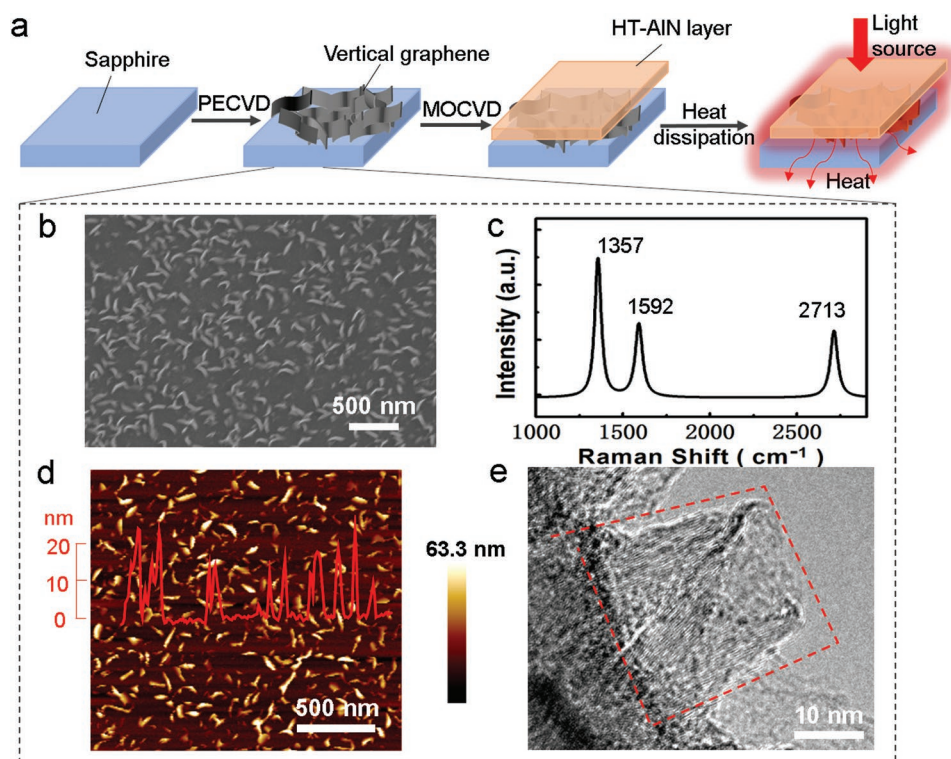
Figure 1. Enhancement of the heat dissipation in an AlN film on an Al_2O_3 substrate buffered with VG nanowalls. a) Schematic illustration of heat dissipation enhancement in the $AlN-VG-Al_2O_3$ heterostructures. First, VG nanowalls are grown on a sapphire substrate by PECVD. Then, a mirror-like smooth AlN film is grown on the VG-sapphire substrate by MOCVD. Under illumination, the generated heat can be removed quickly due to the unique structure of the VG nanowalls. b) SEM characterization showing the VG nanowalls, partially covers the surface of sapphire substrate. c) Raman spectroscopy showing three typical peaks at 1357 cm^{-1} (D band), 1592 cm^{-1} (G band), and 2713 cm^{-1} (2D band). d) AFM characterization. The inset shows a height profile of the AFM image, with an average height ≈20 nm. e) A representative cross-sectional TEM image of a vertical graphene nanosheet with ≈22 nm in height.

fabrication time and reduce the cost of production. It should be noted that further increasing the VG coverage (high-density) degrades the crystal quality of the AlN film due to the generation of high density dislocations evidenced by the XRD characterizations in Figure S7, Supporting Information. Therefore, the coverage (density) of VG nanowalls should be optimized for the LED applications.

It is well known that graphene shows good thermal conductivity in the horizontal direction (in plane) but poor thermal conductivity in the vertical direction (out of plane) because of the weak van der Waals interactions between the layers. In contrast to common horizontal graphene, vertical graphene nanowalls present better thermal conductivity in the vertical direction due to their unique 3D structure. Using the traditional Raman method,[23,24,35–37] the thermal conductivity of a suspended vertical graphene nanowall buffer layer is measured to be 0.68×10^3 W m^{-1} K^{-1} (see experimental details in Figures S8–S10, Supporting Information), which is much higher than those of the GaN (130 W m^{-1} K^{-1}), SiC (200 W m^{-1} K^{-1}), and copper (400 W m^{-1} K^{-1}) materials normally used for heat dissipation enhancement in LED devices.[38]

Then, we can evaluate the heat dissipation ability of a VG nanowall-buffered AlN film on sapphire substrates and compare it with that on bare sapphires. Our designed experiments are shown in Figure 1a. **Figure 3**a,c shows schematic illustrations

of the cross-sectional view of the $AlN-Al_2O_3$ and $AlN-VG-Al_2O_3$ structures. Initially, we maintained the same temperature for the two samples. Under the same irradiation with a 1450 nm laser at a power of 850 mW cm^{-2}, the temperatures of both samples quickly increase when the laser is turned on and then gradually increase after 1 min as shown in Figure 3e (more detailed information can be seen in Figures S11–S13, Supporting Information). The surface temperatures of the $AlN-Al_2O_3$ sample and the $AlN-VG-Al_2O_3$ sample presented similar trends versus the irradiation time. However, the surface temperature of $AlN-VG-Al_2O_3$ is the lower of the two. Particularly, after laser exposure for 5 min, the peak temperature detected for the AlN film buffered with vertical graphene nanowalls is 36.7 °C, which is approximately 1.4 °C lower than that of the film without VG nanowalls. After turning the laser off, the temperatures of both samples decrease gradually. A histogram of the statistics of the measured heating and cooling rates for the $AlN-Al_2O_3$ sample and $AlN-VG-Al_2O_3$ sample are shown in Figure 3f, indicating more effective thermal transport during the heating and cooling processes for the $AlN-VG-Al_2O_3$ sample due to the existence of the VG nanowalls.

To quantitatively evaluate the effect of the vertical graphene nanowalls between sapphire and AlN on the heat dissipation, a 2D simulation of the temperature distribution based on finite element analysis was carried out (Figure 3b,d;
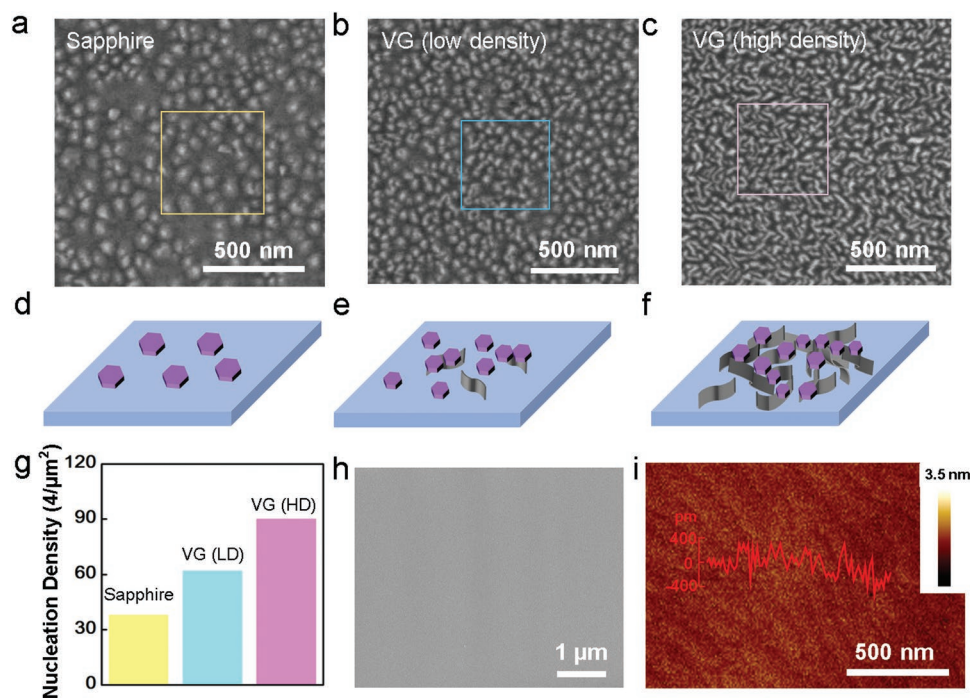
Figure 2. Effects of the VG nanowall buffer layer on the nucleation and quality of the AlN film grown on the Al_2O_3 substrate. a–c) At the initial nucleation stage, SEM images of the AlN on the bare sapphire substrate (a), the substrate with a low density of VG nanowalls (b), and the substrate with a high density of VG nanowalls (c). d–f) The corresponding schematic illustrations of the initial AlN nucleation conditions on the different substrates. On the sapphire substrate, only several AlN nucleation islands are formed. On the low-density VG nanowall-sapphire substrate, AlN nucleates on the bare sapphire or at the edges of the VG nanowalls. On the high-density VG nanowall sapphire substrate, AlN primarily nucleates on the edges of the VG nanowalls. g) The statistics for the number of AlN nucleation sites in a 500 nm × 500 nm area as plotted from (a)–(c). h) SEM and i) AFM images of a flat AlN film grown on a low density VG nanowall substrate, showing atomically flat feature with RMS roughness ≈1.8 Å. The inset in (i) shows the height profile of the AFM image, confirming its flatness at the atomic scale.

Figure S14, Supporting Information). Two structures based on the real sample configurations were constructed. The AlN-Al_2O_3 structure consists of a 1 cm (length) × 300 µm (height) sapphire layer and 1 cm (length) × 2 µm (height) AlN layer. For the simulated AlN-VG-Al_2O_3 structure, in addition to the structure mentioned above, approximately 8×10^4 VG nanowalls per cm, which were 20 nm in height and 20 nm in length, were distributed at regular intervals (an interval of 100 nm) between the sapphire layer and AlN layer. A Gaussian-distributed heat source with a 10 W central heat flux and 2 mm radius laser spot was used to simulate the laser source. In the calculations, to better predict the maximum temperature, mesh gridding was performed using a triangular mesh: for the AlN layer, the minimum side of each triangle unit is 0.02–0.5 µm; for the VG nanowall layer, the minimum side is 2–10 nm; and for the Al_2O_3 layer, the minimum side is 1–10 µm. As a result, after 5 min of laser irradiation, the peak temperature in the sample with VG nanowalls is 35.97 °C, compared to 37.65 °C (exhibiting 1.68 °C higher) for the AlN layer on bare sapphire, which is in excellent agreement with the experimental results. Therefore, the temperature difference can effectively lower the junction temperature of the LEDs, thereby improving the light output power and enhancing the stability and life of the devices.[39–41]

Furthermore, with the help of the VG nanowall buffer layer, we find that the strain in the AlN layer can be largely relieved. The vibrational properties that are sensitive to the strain conditions[27] are shown in **Figure 4**, Figures S15 and S16 and

Table S1, Supporting Information. For AlN on bare sapphire, the strain comes from the large lattice mismatch and significant difference in thermal coefficients between the nitride and sapphire substrates, for which the thermal expansion coefficients of AlN and Al_2O_3 are $4.2–5.3 \times 10^{-6}$ and $7.5–8.5 \times 10^{-6}$ K^{-1}, respectively.[42] As a consequence of AlN having a smaller thermal expansion coefficient than Al_2O_3, the compressive stress in AlN was normally generated during the cooling process from the high growth temperature to room temperature. Effectively releasing the strain in the AlN film can play an important role in reducing the polarization, improving the hole and electron overlapping, increasing the internal quantum efficiency, and enhancing the luminous efficiency of LED devices.[43]

Changes in the Raman frequencies are usually used to analyze the strain in AlN/GaN materials.[44] Particularly, for AlN, the E_2 (high) mode can be used to detect the stress along the c plane of AlN.[45–47] For the epitaxial growth of AlN on a sapphire substrate, the E_2 (high) mode is usually higher than that of a strain-free bulk AlN sample. Compared to the AlN film on bare sapphire, the Raman frequencies of AlN films with different types of buffer layers (i.e., horizontal graphene and vertically oriented graphene) are lower, suggesting all these buffer layers are helpful for strain relaxation (Figure 4a,b).[48,49] Among them, the AlN-VG-Al_2O_3 structure has the lowest frequency at ≈657.4 ± 0.2 cm^{-1}, which is very close to 657.4 cm^{-1} for strain-free bulk AlN,[44] indicating that the VG nanowall buffer layer is very effective at releasing the strain.
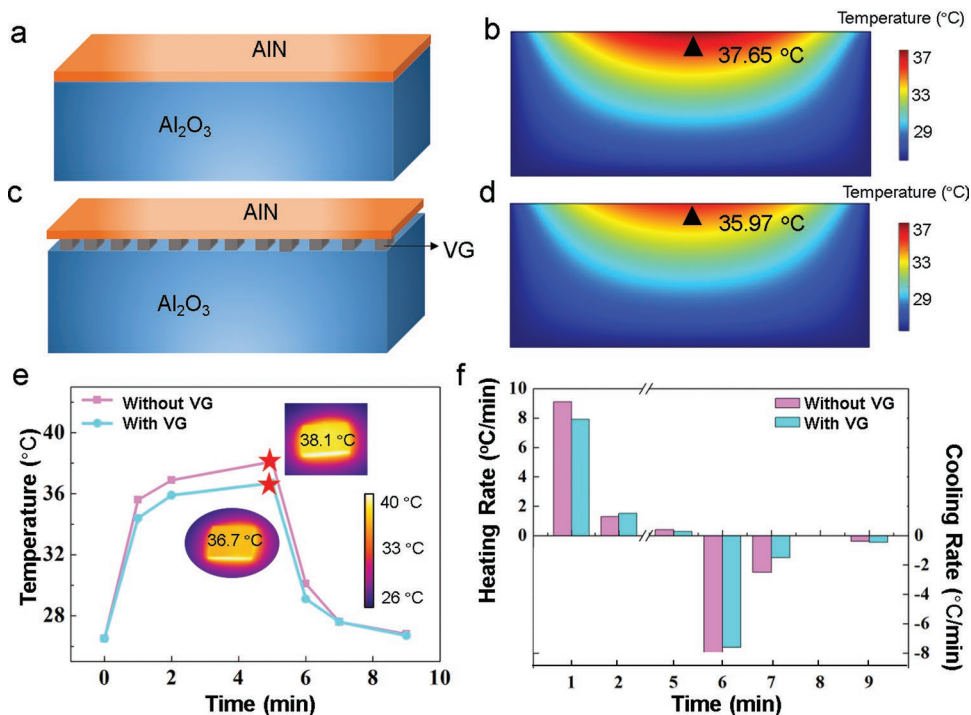
Figure 3. Heat dissipation in an AlN film on an Al_2O_3 substrate with and without VG nanowalls. a,c) Schematic illustrations of an AlN-Al_2O_3 structure (a) and an AlN-VG-Al_2O_3 structure (c). b,d) Simulated 2D distributions of the heat mapping of an AlN-Al_2O_3 cross-section (b) and an AlN-VG-Al_2O_3 cross-section (d). e) The measured temperatures of AlN-Al_2O_3 and AlN-VG-Al_2O_3 are plotted as a function of the time as detected by an infrared thermal imaging camera. The insets show the temperature distributions under laser irradiation for 5 min. f) The calculations for the heating rate and cooling rate versus time ($\Delta T/\Delta t$) for the AlN-Al_2O_3 and AlN-VG-Al_2O_3 samples.
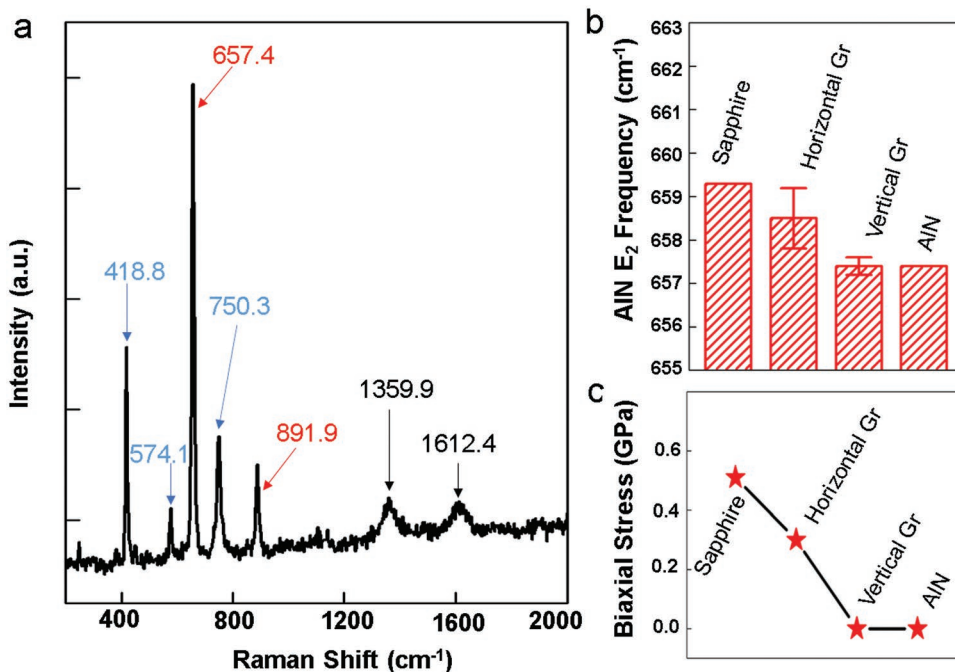
Figure 4. Raman characterization of the as-grown AlN-VG-Al_2O_3 heterostructures. a) A representative Raman spectrum of the sample after the growth of an AlN film on an Al_2O_3 substrate buffered with the VG nanowalls. The Raman characterization confirms the existence of AlN, VG nanowalls, and Al_2O_3 concurrently. b) The E_2 (high) Raman frequency of AlN obtained on sapphire, horizontal graphene-sapphire, VG nanowall-sapphire, and bulk AlN substrates. c) The corresponding biaxial stress for bulk AlN (657.4 cm^{-1}) and AlN films on sapphire substrates with different types of buffer layers.

**ADVANCED
SCIENCE NEWS**

www.advancedsciencenews.com

**ADVANCED
MATERIALS**

www.advmat.de
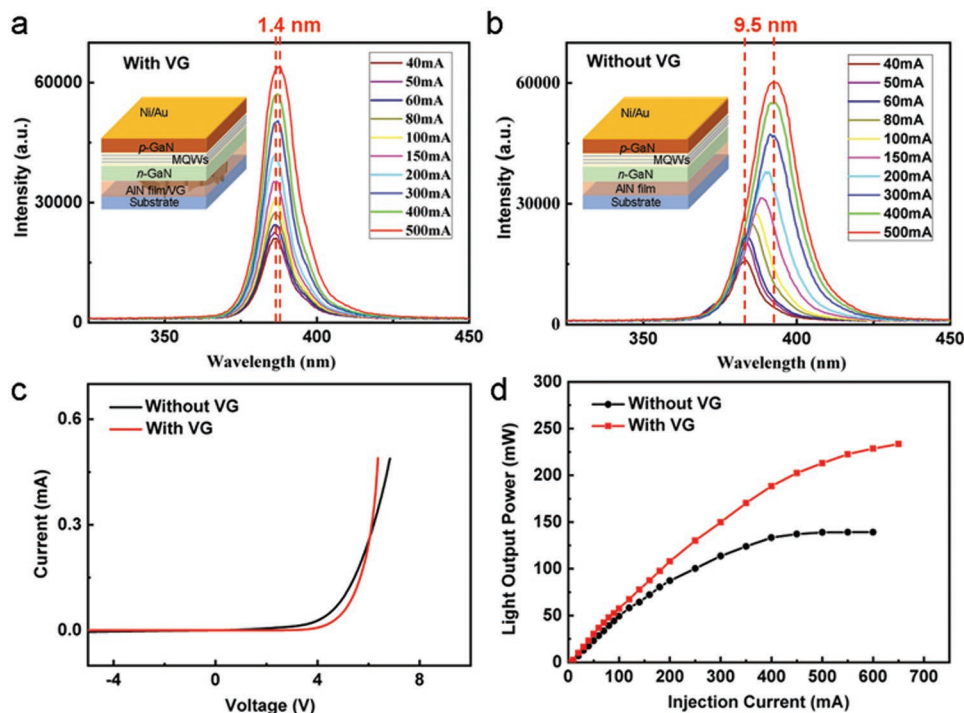
Figure 5. Application of the as-grown VG-nanowall/sapphire in UV-LEDs. a,b) EL spectra of the UV-LEDs with (a) VG nanowalls and without (b) VG nanowalls measured by varying the injection current from 40 to 500 mA. The insets in (a) and (b) are schematic diagrams of the InGaN-based UV-LED structure for the AlN/VG-nanowall/sapphire and AlN/sapphire substrates. c) I–V characterization curves of the UV-LEDs fabricated with VG nanowalls and without VG nanowalls. d) Light output power of the UV-LEDs fabricated with VG nanowalls and without VG nanowalls as a function of the injection current.

We can also quantitatively analyze the stress based on the shift of the Raman frequency of the E_2 (high) mode for AlN: $\sigma_\alpha = \Delta\omega[E_2(\text{high})]/\kappa$, where $\Delta\omega[E_2(\text{high})]$ is the strain-induced Raman frequency shift of the E_2 peak, and the coefficient $\kappa = 3.7$ cm^{-1} GPa^{-1}.[34] The calculated biaxial stress of the AlN layer for the different samples is shown in Figure 4c. The AlN layer on the sapphire substrate suffered from a 0.51 GPa compressive stress, while the residual stress is almost reduced to zero when VG nanowalls are included as an interlayer. Furthermore, with the inclusion of VG nanowalls, the strain in the sapphire substrate is also affected, and in turn, the growth of the AlN film also changes the strain conditions of the VG nanowalls. These details are included in the Supporting Information.

InGaN-based UV-LED structures were fabricated on the as-grown AlN/VG-nanowall/sapphire substrate (schematically shown in the inset of **Figure 5**a) and AlN/sapphire substrate (schematically shown in the inset of Figure 5b). Figure 5a,b shows the electroluminescence (EL) characteristics of the fabricated LEDs with VG nanowalls and without VG nanowalls. The EL peak wavelength of the LED using VG nanowalls as a buffer layer shows a 1.4 nm shift as the applied current increases from 40 to 500 mA, obviously reducing the wavelength shift compared to that of the LED not using a VG buffer layer (9.5 nm). The different current–voltage (I–V) characterization curves in Figure 5c indicate a turn-on voltage of approximately 3.2 V for the 390 nm UV-LED device, confirming the better quality of the LED device with the VG nanowalls as a buffer layer. Figure 5d shows the light output power (LOP) curves of the related two LED devices as a function of the injection current.

For the LED device without a VG buffer layer, the saturated LOP is 137 mW at an injection current of 450 mA. However, for the LED device with a VG buffer layer, the LOP is 200 mW at 450 mA and still increases with increasing injection current (i.e., 230 mW at 600 mA). The external quantum efficiency is increased ≈33.33% due to the presence of VG nanowalls under 350 mA current. Moreover, the smaller EL peak wavelength shift and higher saturation injection current can be explained in terms of the better heat dissipation and strain relieving effects of the VG nanowalls.

In summary, we propose a scheme for improving the heat dissipation of an AlN film, taking advantage of the unique 3D structure and good thermal conductivity of VG nanowalls. Through the MOCVD growth of an AlN film on a sapphire substrate buffered with VG nanowalls, an atomically flat single-crystal AlN film with low density of dislocations can be obtained. The experimental results confirm that the VG nanowalls can play important roles in AlN nucleation and strain release. Compared to the AlN film grown on the bare Al_2O_3 substrate, AlN grown on the VG-Al_2O_3 substrate exhibits an approximately 1.4 °C lower temperature under irradiation with a laser light due to the enhanced heat dissipation. High-performance InGaN-based UV-LED devices were also fabricated on a VG nanowall-sapphire substrate, which benefited from the strain released from the AlN film and the perfect thermal conductivity of the VG nanowalls. Thus, the LED fabricated on the VG-sapphire substrate shows a 37% improvement in the light output power under a high injection current (350 mA) with an effective 3.8% temperature reduction. Through both

experimental and theoretical analysis, we conclude that the VG nanowall buffer layer can be used as a good material for heat dissipation enhancement, which provides a new strategy to resolve heat problems in LED applications.

Experimental Section

Vertically Oriented Graphene Nanowalls Growth: The growth of vertically oriented graphene nanowalls on sapphire substrate was carried out in a dc-PECVD system (AIXTRON, Black Magic 6-inch). The growth temperature is ≈580 °C with 1000 sccm Ar and 2 sccm CH_4 being introduced into the system. Generally, horizontally oriented graphene can be obtained by CVD process. In this work, by taking advantage of the vertical electric field generated in the dc-PECVD system, graphene prefers to grow with vertical orientation.[29]

AlN Growth: AlN film was grown by one-step high temperature MOCVD, using trimethylaluminum (TMAl) (70 sccm) and NH_3 (500 sccm) as Al and N precursors and H_2 (12 SLM) as the carrier gas. The growth time is about 2 h at a nominal temperature of 1200 °C.

UV-LED Device Fabrication: u-GaN layer was grown at 1045 °C for 55 min with the NH_3 flow of 6000 sccm and trimethylgallium (TMGa) flow of 80 sccm, respectively, followed by an n-doped GaN layer with the silane flow of 2.34 sccm. Then five periods of $In_xGa_{1−x}N$/GaN active layer was grown at 735 °C/834 °C with 3 nm InGaN well layers and 12 nm GaN barriers. The active layer was capped with a p-GaN layer deposited at 950 °C with the bis-cyclopentadienyl magnesium (Cp_2Mg) flow of 120 sccm, followed by an annealing process at 720 °C for 10 min under N_2 ambient.

Thermal Conductivity Measurement: Taking advantage of the self-supportive property of VG nanowalls, VG nanowalls layer could be directly transferred onto 40 μm-diameter copper grids without carbon film. Then the thermal conductivity of VG nanowalls can be measured based on micro-Raman spectroscopy (Supporting Information).

Characterization: The morphology and structure of the grown VG nanowalls on sapphire substrate were characterized with SEM (Hitachi S-4800, acceleration voltage 5–30 kV), Raman spectrum (Horiba, LabRAM HR-800, 514 nm laser wavelength, ×100 objective) (WITec alpha300 RS), AFM (Bruker Dimension Icon), and TEM (FEI Tecnai F20, acceleration voltage 200 kV). The XRD was measured with Rigaku (D/MAX 2500 PC). The temperature was detected by infrared imaging system (BM_IR V7.4).

Supporting Information

Supporting Information is available from the Wiley Online Library or from the author.

Acknowledgements

Conflict of Interest

The authors declare no conflict of interest.

Keywords

[1] S. Pimputkar, J. Speck, S. P. DenBaars, S. Nakamura, *Nat. Photonics* **2009**, *3*, 180.

[2] E. F. Schubert, J. K. Kim, *Science* **2005**, *308*, 1274.

[3] S. Choi, H. J. Kim, J. Liu, J. Kim, J. H. Ryou, R. D. Dupuis, A. M. Fischer, F. A. Ponce, *Appl. Phys. Lett.* **2010**, *96*, 221105.

[4] Y. Kobayashi, K. Kumakura, T. Akasaka, T. Makimoto, *Nature* **2012**, *484*, 223.

[5] J. Li, Z. Y. Fan, R. Dahal, M. L. Nakarmi, J. Y. Lin, H. X. Jiang, *Appl. Phys. Lett.* **2006**, *89*, 213510.

[6] A. Khan, K. Balakrishnan, T. Katona, *Nat. Photonics* **2008**, *2*, 77.

[7] R. Gutt, T. Passow, M. Kunzer, W. Pletschen, L. Kirste, K. Forghani, F. Scholz, K. Köhler, J. Wagner, *Appl. Phys. Express* **2012**, *5*, 032101.

[8] G. Harbers, G. Mueller, L. Zhou, M. G. Craford, M. R. Krames, O. B. Shchekin, R. Muellermach, *J. Display Technol.* **2007**, *3*, 98.

[9] R. H. Horng, J. S. Hong, Y. L. Tsai, D. S. Wuu, C. M. Chen, C. J. Chen, *IEEE Trans. Electron Devices* **2010**, *57*, 2203.

[10] T. B. Wei, K. Wu, Y. Chen, J. Yu, Q. Yan, Y. Y. Zhang, R. Duan, J. Wang, Y. Zeng, J. M. Li, *IEEE Electron Device Lett.* **2012**, *33*, 857.

[11] O. B. Shchekin, J. E. Epler, T. A. Trottier, T. Margalith, D. A. Steigerwald, M. O. Holcomb, P. S. Martin, M. R. Krames, *Appl. Phys. Lett.* **2006**, *89*, 071109.

[12] C.-F. Chu, F.-I. Lai, J.-T. Chu, C.-C. Yu, C.-F. Lin, H.-C. Kuo, S. C. Wang, *J. Appl. Phys.* **2004**, *95*, 3916.

[13] R.-H. Horng, W.-C. Kao, S.-L. Ou, D.-S. Wuu, *Appl. Phys. Lett.* **2012**, *101*, 171102.

[14] X. A. Cao, S. D. Arthur, *Appl. Phys. Lett.* **2004**, *85*, 3971.

[15] A. A. Balandin, *Nat. Mater.* **2011**, *10*, 569.

[16] K. S. Novoselov, V. I. Fal'ko, L. Colombo, P. R. Gellert, M. G. Schwab, K. Kim, *Nature* **2012**, *490*, 192.

[17] S. Subrina, D. Kotchetkov, A. A. Balandin, *IEEE Electron Device Lett.* **2009**, *30*, 1281.

[18] J. Kang, H. Kim, K. S. Kim, S.-K. Lee, S. Bae, J.-H. Ahn, Y.-J. Kim, J.-B. Choi, B. H. Hong, *Nano Lett.* **2011**, *11*, 5154.

[19] K. Chung, C. H. Lee, G. C. Yi, *Science* **2010**, *330*, 655.

[20] S. J. Kwon, T.-H. Han, T. Y. Ko, N. Li, Y. Kim, D. J. Kim, S.-H. Bae, Y. Yang, B. H. Hong, K. S. Kim, S. Ryu, T. W. Lee, *Nat. Commun.* **2018**, *9*, 2037.

[21] A. A. Balandin, S. Ghosh, W. Bao, I. Calizo, D. Teweldebrhan, F. Miao, C. N. Lau, *Nano Lett.* **2008**, *8*, 902.

[22] H. Li, H. Ying, X. Chen, D. L. Nika, A. I. Cocemasov, W. Cai, A. A. Balandin, S. Chen, *Nanoscale* **2014**, *6*, 13402.

[23] Z. Bo, Y. Yang, J. Chen, K. Yu, J. Yan, K. Cen, *Nanoscale* **2013**, *5*, 5180.

[24] H. Yan, Y. Tang, W. Long, Y. Li, *J. Mater. Sci.* **2014**, *49*, 5256.

[25] J. R. Grandusky, J. F. Chen, S. R. Gibb, M. C. Mendrick, C. G. Moe, L. Rodak, G. A. Garrett, M. Wraback, L. J. Schowalter, *Appl. Phys. Express* **2013**, *6*, 032101.

[26] H. Chang, Z. Chen, W. Li, J. Yan, R. Hou, S. Yang, Z. Liu, G. Yuan, J. Wang, J. Li, P. Gao, T. Wei, *Appl. Phys. Lett.* **2019**, *114*, 091107.

[27] V. Darakchieva, J. Birch, M. Schubert, T. Paskova, S. Tungasmita, G. Wagner, A. Kasic, B. Monemar, *Phys. Rev. B* **2004**, *70*, 045411.

[28] L. Liu, B. Liu, J. H. Edgar, S. Rajasingam, M. Kuball, *J. Appl. Phys.* **2002**, *92*, 5183.

[29] H. Ci, H. Ren, Y. Qi, X. Chen, Z. Chen, J. Zhang, Y. Zhang, Z. Liu, *Nano Res.* **2018**, *11*, 3106.

[30] Y. Wu, B. Yang, *Nano Lett.* **2002**, *2*, 355.

[31] Y. Wu, B. Yang, B. Zong, H. Sun, Z. Shen, Y. Feng, *J. Mater. Chem.* **2004**, *14*, 469.

[32] M. Zhu, J. Wang, B. C. Holloway, R. A. Outlaw, X. Zhao, K. Hou, V. Shutthanandan, D. M. Manos, *Carbon* **2007**, *45*, 2229.

[33] Z. H. Ni, H. M. Fan, Y. P. Feng, Z. X. Shen, B. J. Yang, Y. H. Wu, *J. Chem. Phys.* **2006**, *124*, 204703.

[34] Y. Li, Y. Zhao, T. Wei, Z. Liu, R. Duan, Y. Wang, X. Zhang, Q. Wu, J. Yan, X. Yi, G. Yuan, J. Wang, J. Li, *Jpn. J. Appl. Phys.* **2017**, *56*, 085506.

[35] S. Chen, A. L. Moore, W. Cai, J. W. Suk, J. An, C. Mishra, C. Amos, C. W. Magnuson, J. Kang, L. Shi, *ACS Nano* **2011**, *5*, 321.

[36] C. Faugeras, B. Faugeras, M. Orlita, M. Potemski, R. R. Nair, A. K. Geim, *ACS Nano* **2010**, *4*, 1889.

[37] W. Cai, A. L. Moore, Y. Zhu, X. Li, S. Chen, L. Shi, R. S. Ruoff, *Nano Lett.* **2010**, *10*, 1645.

[38] P. Y. Tsai, H. K. Huang, C.-M. Sung, M. C. Kan, Y. H. Wang, *IEEE Electron Device Lett.* **2013**, *34*, 1029.

[39] N. Narendran, Y. M. Gu, *J. Display Technol.* **2005**, *1*, 167.

[40] N. Han, T. V. Cuong, M. Han, B. D. Ryu, S. Chandramohan, J. B. Park, J. H. Kang, Y. J. Park, K. B. Ko, H. Y. Kim, *Nat. Commun.* **2013**, *4*, 1452.

[41] S. H. Lee, X. Y. Guan, S. K. Jeon, J. S. Yu, *Phys. Status Solidi A* **2016**, *213*, 46.

[42] H. Harima, *J. Phys.: Condens. Matter* **2002**, *14*, R967.

[43] C. Kisielowski, J. Krüger, S. Ruvimov, T. Suski, E. Jones, Z. Liliental-Weber, M. Rubin, E. R. Weber, M. D. Bremser, *Phys. Rev. B* **1996**, *54*, 17745.

[44] M. Kuball, *Surf. Interface Anal.* **2001**, *31*, 987.

[45] T. Prokofyeva, M. Seon, J. Vanbuskirk, M. Holtz, S. A. Nikishin, N. N. Faleev, H. Temkin, S. Zollner, *Phys. Rev. B* **2001**, *63*, 125313.

[46] H. J. Trodahl, F. Martin, P. Muralt, N. Setter, *Appl. Phys. Lett.* **2006**, *89*, 061905.

[47] A. Sarua, M. Kuball, J. E. Van Nostrand, *Appl. Phys. Lett.* **2002**, *81*, 1426.

[48] Z. Chen, X. Zhang, Z. Dou, T. Wei, Z. Liu, Y. Qi, H. Ci, Y. Wang, Y. Li, H. Chang, J. Yan, S. Yang, Y. Zhang, J. Wang, P. Gao, J. Li, Z. Liu, *Adv. Mater.* **2018**, *30*, 1801608.

[49] Y. Qi, Y. Wang, Z. Pang, Z. Dou, T. Wei, P. Gao, S. Zhang, X. Xu, Z. Chang, B. Deng, S. Chen, Z. Chen, H. Ci, R. Wang, F. Zhao, J. Yan, X. Yi, K. Liu, H. Peng, Z. Liu, L. Tong, J. Zhang, Y. Wei, J. Li, Z. Liu, *J. Am. Chem. Soc.* **2018**, *140*, 11935.

1901624 (8 of 8)